Science of the Total Environment 437 (2012) 331–338

Contents lists available at SciVerse ScienceDirect

Science of the Total Environment

journal homepage: www.elsevier.com/locate/scitotenv

Characterization of coal fly ash nanoparticles and induced oxidative DNA damage in human peripheral blood mononuclear cells

Sourabh Dwivedi [a,1], Quaiser Saquib [a,1], Abdulaziz A. Al-Khedhairy [a], Al-Yousef Sulaiman Ali [b], Javed Musarrat [a,c,*]

[a] Department of Zoology, College of Science, King Saud University, P.O. Box 2455, Riyadh 11451, Saudi Arabia
[b] Department of Medical Laboratory Sciences, College of Applied Medical Science, University of Dammam, P.O. Box 1683, Hafr Al Batin-31991, Saudi Arabia
[c] Department of Agricultural Microbiology, Faculty of Agricultural Sciences, AMU, Aligarh202002, India

HIGHLIGHTS

- CFA consists of spherical crystalline nanoparticles in size range of 11–25 nm.
- Alkaline unwinding assay revealed single-strandedness in CFA treated ctDNA.
- CFA nanoparticles exhibited the ability to induce ROS and oxidative DNA damage.
- Comet and CBMN assays revealed DNA and chromosomal breakage in PBMN cells.
- CFA-NPs resulted in mitochondrial membrane damage in PBMN cells.

ARTICLE INFO

Article history:
Received 5 June 2012
Received in revised form 25 July 2012
Accepted 1 August 2012
Available online xxxx

Keywords:
Coal fly ash
Nanoparticles
XRD
Reactive oxygen species
Genotoxicity

ABSTRACT

The nano-sized particles present in coal fly ash (CFA) were characterized through the X-ray diffraction (XRD), transmission and scanning electron microscopy (TEM, SEM), atomic force microscopy (AFM) and Fourier transform infrared spectroscopy (FTIR) analyses. The XRD data revealed the average crystallite size of the CFA nanoparticles (CFA-NPs) as 14 nm. TEM and SEM imaging demonstrated predominantly spherical and some polymorphic structures in the size range of 11 to 25 nm. The amount of heavy metal associated with CFA particles (μg/g) were determined as Fe (34160.0 ± 1.38), Ni (150.8 ± 0.78), Cu (99.3 ± 0.56) and Cr (64.0 ± 0.86). However, the bioavailability of heavy metals in terms of percent release was in the order as Cr > Ni > Cu > Fe in CFA-dimethyl sulfoxide (DMSO) extract. The comet and cytokinesis blocked micronucleus (CBMN) assays revealed substantial genomic DNA damage in peripheral blood mononuclear (PBMN) cells treated with CFA-NPs in Aq and DMSO extracts. About 1.8 and 3.6 strand breaks per unit of DNA were estimated through alkaline unwinding assay at 1:100 DNA nucleotide/CFA ppm ratios with the Aq and DMSO extracts, respectively. The DNA and mitochondrial damage was invariably greater with CFA-DMSO extract vis-à-vis -Aq extract. Generation of superoxide anions ($O_2^{\bullet -}$) and intracellular reactive oxygen species (ROS) through metal redox-cycling, alteration in mitochondrial potential and 8-oxodG production elucidated CFA-NPs induced oxidative stress as a plausible mechanism for CFA-induced genotoxicity.

1. Introduction

The world-wide consumption of coal, to meet the global primary energy requirements, is expected to increase by 1.9% per year, with concurrent increase in the production of fly ash. Currently, the annual production rate of coal fly ash (CFA) in the United States and Europe is about 67.7 million tons and 40.4 thousand metric tons, respectively (www.rmajko.com). In India, the thermal power plants produce an estimated 100 million tons of fly ash per year (Manerikar et al., 2008). About 80% of this fly ash is released into 65,000 acres of land used as ash ponds (Singh and Siddiqui, 2003; Jala and Goyal, 2006; Pandey and Singh, 2010). Such a heavy discharge of fly ash eventually causes serious environmental pollution and health hazards, due to the presence of surface bound hydrocarbons and toxic metals (Kalra et al., 1998; Zhou et al., 2005; Parisar, 2007). Heavy metals such as Cu, Pb, Cd, Cr, Zn and Ni (Bauser et al., 1978; Griffin et al., 1980; Tiwari et al., 2008) in fly ash are reported to exert adverse effects on aquatic and terrestrial ecosystems (Adriano et al., 1980; Wong and Wong, 1990; Ali et al., 2004). Recently, Di Pietro et al. (2009, 2011a) demonstrated that the transition metals adsorbed to oil fly ash (OFA) cause DNA damage, lipid peroxidation and mitochondrial

* Corresponding author at: Department of Zoology, College of Science, King Saud University, P.O. Box 2455, Riyadh 11451, Saudi Arabia. Tel.: +966 1 4675768.
E-mail address: musarratj1@yahoo.com (J. Musarrat).
[1] These authors contributed equally to this work.

0048-9697/$ – see front matter © 2012 Elsevier B.V. All rights reserved.
http://dx.doi.org/10.1016/j.scitotenv.2012.08.004

dysfunction in cultured human epithelial alveolar (A549) cells. Mainly, the Fe(III) and V(IV) were found responsible for the mitochondrial alterations in pneumocytes exposed to OFA (Di Pietro et al., 2011a). Also, the transition metals in fine particulate matter generated by combustion induce oxidative DNA damage and inflammation (Di Pietro et al., 2011b).

Several toxicological studies with airborne particulate matter and OFA have been performed on various organisms including human pneumocytes and lymphocytes (Fujii, et al., 2001; Chen et al., 2010; Di Pietro et al., 2009, 2011a,b,). Recently, Markad et al. (2012) demonstrated the fly ash induced DNA damage and DNA–protein crosslinks in earthworm coelomocytes through comet assay. Also, the mutagenicity of ultrasonically treated DMSO extract of ESP fly ash in *Salmonella* tester strains TA97 and TA102, and chromosome damage in lymphocytes of humans exposed to both ESP fly ash and Lytag have been reported (Kleinjans et al., 1989). However, still the information is limited on coal fly ash nanoparticles (CFA-NPs) with respect to their characterization, surface associated transition metals and their genotoxic effects in humans. Earlier studies have not adequately considered the fine CFA particle characteristics and mechanistic aspect of the CFA-induced genotoxicity, in terms of DNA strand breaks, ROS production and oxidative damage in human PBMN cells. Therefore, in view of extensive production of CFA and its wider applications, and genotoxic risk to humans, it is considered important to investigate the average particle size of CFA-NPs, and their toxicity evaluation at cellular and molecular level. Since, the nano-sized particles provide larger surface area for binding of chemicals including xenobiotics and transition metals, and can easily enter into cells (Donaldson et al., 2003; Gwinn and Vallyathan, 2006; Duffin et al., 2007; Saquib et al., 2012), there is a growing interest in toxicology of nanoparticles and their significance in relation to human health. This has prompted us to characterize the CFA-NPs using sensitive techniques like X ray diffraction (XRD), Fourier transform infra red spectroscopy (FTIR), transmission and scanning electron microscopy (TEM, SEM) and atomic force microscopy (AFM). The study elucidates the role of CFA-NPs induced reactive oxygen species (ROS) in causing DNA strand breaks, oxidative lesions (8-oxodG), and chromosomal breaks (micronuclei formation) in cultured human peripheral blood mononuclear (PBMN) cells.

2. Materials and methods

2.1. Sampling of CFA

CFA were collected at a depth of 10–15 cm from the dumping site of Harduaganj thermal power plant, located (28°01′N 78°07′E/28.0175°N 78.13°E) around 18 km North-East of Aligarh district, India. This power plant consumes 3192 tons of bituminous coal/day and produces 650 tons/day of fly ash. Samples from ten different locations at the same site were mixed thoroughly to obtain a composite sample, representative of the test region and stored at 4 °C for subsequent analysis.

2.2. Preparation of CFA aqueous (Aq) and DMSO extracts

The CFA extracts were prepared by mixing 1 g of air dried CFA in 100 ml of ultrapure water and culture grade DMSO (0.5%), separately in 250 ml flasks. Both flasks were kept on a rotary shaker at 25 °C for 24 h. The suspensions were then sonicated using an ultrasonicator (Pro Scientific, Inc., USA) and centrifuged at 11,739×*g* for 30 min. The supernatants (extracts) were carefully aspirated, and filtered through 0.22 μm syringe filter. The filtered extracts were stored at −20 °C in 2 ml aliquots and used for the toxicity studies.

2.3. Analysis of CFA samples for presence of heavy metals

The powdered CFA and its aqueous (Aq) and DMSO extracts were analyzed for heavy metals such as chromium (Cr), copper (Cu), iron (Fe) and nickel (Ni). In brief, 1 g air dried CFA was mixed with 5 ml of 70% HNO_3 and 2 ml hydrofluoric acid and digested on a heating plate for 1 h at 180 °C, following the method described earlier (Sushil and Batra, 2006). The digested samples were filtered through Whatman No. 1 filter paper and transferred to pre-labeled volumetric flasks to make up the volume up to 100 ml with ultrapure water. The Aq and DMSO (0.5%) extracts were sonicated prior to analysis and directly analyzed for heavy metals by use of an atomic absorption spectrophotometer (GBC 932 plus, Australia).

2.4. X-ray diffraction analysis of CFA

Finely powdered sample of air dried CFA was analyzed using X'pert PRO analytical diffractometer (Almelo, The Netherlands) using CuK_α radiation ($\lambda = 1.54056$ Å) in the range of $20° \leq 2\theta \leq 80°$ at 40 keV. In order to calculate the particle size (D) of CFA sample, the Scherrer's equation ($D = 0.9\lambda/\beta\cos\theta$) has been used (Patterson, 1939), where λ is the wavelength of X-ray, β is the broadening of diffraction line measured as half of its maximum intensity in radians and θ is the Bragg's diffraction angle. The average particle size of CFA was estimated from the line width of the XRD peak.

2.5. Analysis of CFA by transmission electron microscopy (TEM) and scanning electron microscopy (SEM)

TEM analysis of CFA was performed on a transmission electron microscope (Hitachi, H-7500, Japan) at an accelerating voltage of 90 kV. Samples were prepared by drop-coating CFA solutions (1% CFA-DMSO extract) onto carbon-coated gold TEM grids. Film of CFA sample on TEM grid was allowed to stand for 2 min. The extra solution was removed using a blotting paper and the grid was allowed to dry prior to measurement. For SEM analysis, the samples were prepared by dispersing CFA onto a conductive carbon tape. Samples were coated with gold to prevent charging and analyzed by use of scanning electron microscope (JEOL 6400, Japan). The typical acceleration potential used was 15 kV at a beam current of 10^{-9} A.

2.6. Infrared spectroscopy and atomic force microscopy (AFM) of CFA

FTIR was employed for assessment of functional groups on CFA particles. Briefly, the air dried powder of CFA was diluted with spectroscopic grade KBr (mass ratio of about 1:100) and the spectrum was recorded. FTIR measurements were carried out on Interspec 2020 FTIR (Spectrolab, U.K.) in the diffuse reflectance mode at a resolution of 4 cm^{-1} in KBr pellets.

CFA particles were examined using atomic force microscope (Veeco Instruments, USA). Analysis was performed by running the machine in non-contact tapping mode. Characterization of CFA was done by observing the patterns appeared on the surface topography and analyzing the AFM data. Tapping mode imaging was implemented in ambient air by oscillating the cantilever assembly at or near the cantilever's resonant frequency using a piezoelectric crystal. The topographical images were obtained in tapping mode at a resonance frequency of 218 kHz.

2.7. CFA-induced DNA damage

CFA-induced strand breaks in the calf thymus DNA (ctDNA) were quantitated by alkaline unwinding assay using hydroxyapatite batch procedure (Saquib et al., 2009). In brief, the ctDNA (100 μg) in a volume of 0.5 ml in multiple sterile tubes were treated with Aq and DMSO extracts of CFA in range of 1:5 to 1:100 DNA nucleotide/CFA extract ppm ratio. ctDNA treated with DMSO and EMS in the ratio of 1:10 was taken as negative and positive controls, respectively. The treatment was carried out for 30 min at 37 °C. The tubes were immediately placed on ice and subjected to alkaline unwinding by rapid addition of an equal volume of 0.06 N NaOH in 0.01 M Na_2HPO_4, pH 12.5, followed by brief vortexing. Alkaline unwinding was allowed

to complete in dark for 30 min. The pH of the reaction mixture was then neutralized to pH 7.0 with the addition of 0.07 N HCl. Subsequently, 20 μM EDTA containing 2% SDS was added and the resultant mixture was transferred to pre-heated stoppered glass tubes containing 0.5 M potassium phosphate buffer, pH 7.0 and 10% formamide. The samples were incubated at 60 °C for 2 h with intermittent vortexing. The relative amount of duplex and single stranded DNA present at the end of alkaline unwinding was quantitated. Single stranded DNA was selectively eluted from the hydroxyapatite matrix with 0.125 M potassium phosphate buffer, pH 7.0 containing 20% formamide. However, duplex DNA was removed with 0.5 M potassium phosphate buffer, pH 7.0 containing 20% formamide. CFA-induced strand breaks and number of breaks per unit of ctDNA were determined following the algorithm described previously (Saquib et al., 2009).

2.8. CFA-induced 8-oxo-2′-deoxyguanosine (8-oxodG) formation in ctDNA

Varying amounts of ctDNA (500, 1000 and 1500 ng) were treated with Aq and DMSO extracts of CFA (1000 ppm concentrations) and immobilized on a 96 well plate by overnight absorption at 40 °C following the procedure of Hirayama et al. (1996). Methylene blue (100 μM) was used as positive control. The non-specific sites were blocked with 300 μl of blocking solution containing 3% BSA in PBS (Ca^{2+} and Mg^{2+} free). The plates were further incubated at 37 °C for 3 h. Polyclonal goat anti 8-oxodG antibodies (Cat # AHP592; AbD Serotech, UK), 100 μl/well at dilutions of 1:1,000,000 in blocking solution were added and incubated at 37 °C for 2 h. The solution was discarded and the plates were washed twice with (300 μl/well) with PBS containing 0.05% Tween-20. Subsequently, the secondary antibody (Donkey anti-goat IgG:HRP; Cat # STAR88P, AbD Serotech, UK) diluted at 1:25,000 in blocking solution (100 μl/well) was added and incubated for 2 h at 37 °C. After thorough washing, the 50 μl/well of 1× substrate TMB (3,3′,5,5′-Tetramethylbenzidine) was added. The reaction was stopped by the addition of 2M H_2SO_4 (50 μl/well). Absorbance was read at 450 nm on a Multiskan EX reader (Thermo Scientific, USA). The 8-oxodG was quantified using a calibration curve prepared with the commercially available 8-oxodG standard.

2.9. CFA-induced extracellular ROS generation

Superoxide anions ($O_2^{\bullet -}$) were estimated by nitrobluetetrazolium (NBT) reduction assay (Saquib et al., 2010). In brief, the reaction mixture containing 100 mM Tris–HCl buffer (pH 7.2), 50 μM NBT, 100 μM EDTA, 0.06% Triton X-100 was separately mixed with varying concentrations (100, 200, 400, 600 and 800 ppm) of Aq and DMSO extracts of CFA. The tubes containing reaction mixture were exposed to white light (20 W/m^2) for 2 h. Parallel reactions with Aq and DMSO extracts were run in dark and in presence of EDTA (100 μM), used as free-radical quencher. Absorbance of blue color was read at 560 nm using UV–Visible spectrophotometer (GBC Cintra 10e, Australia) and plotted as a function of CFA concentrations.

2.10. CFA-induced intracellular ROS generation and effect on mitochondrial activity in human PBMN cells

Intracellular ROS production was detected by use of fluorescent probe DCFH-DA, according to the method of Saquib et al. (2009). Human PBMN cells (2×10^6) were exposed to varying concentrations (600, 1200 and 2400 ppm) of Aq and DMSO extracts of CFA in complete RPMI 1640 medium. Comparatively higher concentrations were chosen in this experiment to pick up the fluorescence signal of ROS production, as it was too small at lesser concentrations. Cells were cultured for 24 h at 37 °C in the presence of 5% CO_2 in air in a humidified atmosphere chamber of CO_2 incubator (Thermo Scientific, USA). After two washes with cold PBS, the cells were incubated with DCFH-DA (5 μM) for 60 min at 37 °C in dark. Cells were immediately washed twice with PBS and again suspended in 3 ml of PBS. Fluorescence measurements were carried out at ambient temperature on a Shimadzu spectrofluorophotometer (RF5301PC, Japan) equipped with RF 530XPC instrument control software using a quartz cell of 1 cm path length. The fluorescence intensity was recorded at an excitation wavelength of 485 nm and emission wavelength of 525 nm.

Mitochondrial activity was monitored by observing the changes in the fluorescence intensity of mitochondria specific dye rhodamine (Rh123) in human PBMN cells following the method of Saquib et al. (2010). The mitochondrial membrane potential ($\Delta\Psi m$) was determined by the mean fluorescence intensity (FL1-H) at 488 nm of 10,000 cells by use of a flow cytometer (FACSCalibur, Becton Dickinson, USA).

2.11. Alkaline single cell gel electrophoresis (comet assay) of CFA treated human PBMN cells

Comet assay was performed with human PBMN cells following the standard procedure (Singh et al., 1988; Saquib et al., 2009). The cells were treated with varying concentrations (3, 300, 600, 1200, 1800 and 2400 ppm) of both Aq and DMSO extracts of CFA for 3 h at 37 °C. Both untreated and CFA treated cells were suspended in 100 μl PBS and mixed with 100 μl of 1% low melting agarose (LMA). The cell suspension (80 μl) was then layered on one-third frosted slides, pre-coated with 1% normal melting agarose (NMA) and kept at 4 °C for 10 min. After gelling, a layer of 90 μl of LMA (0.5%) was added. The cells were lysed in a lysing solution overnight. After washing with ultrapure water, the slides were subjected to DNA denaturation in cold electrophoresis buffer at 4 °C for 20 min. Electrophoresis was performed at 0.7 V cm^{-1} for 30 min (300 mA, 24 V) at 4 °C. The slides were then washed three times with neutralization buffer. The slides were stained with ethidium bromide for 5 min and analyzed at 40× magnification using a fluorescence microscope (Nikon ECLIPSE E80i, Japan) coupled with a charge coupled device (CCD) camera. Images from 50 cells (25 from each replicate slide) were randomly selected and subjected to image analysis using software Comet Assay IV (Perceptive Instruments, UK).

2.12. Cytokinesis blocked micronucleus (CBMN) assay of CFA treated human PBMN cells

The CBMN assay was preformed following the methods of Kalantzi et al. (2004) and Saquib et al. (2009). Heparinized blood was obtained by venipuncture from the volunteer. Blood (0.5 ml) was added to 4.5 ml of complete RPMI 1640 medium supplemented with 20% heat-inactivated FBS, 7.5 μg/ml of phytohemagglutinin-M and varying concentrations (600, 1200 and 2400 ppm) of CFA-Aq and -DMSO extracts. The cells were incubated at 37 °C in presence of 5% CO_2 for 24 h. Cells were then pelleted and resuspended in complete medium without CFA. Cytokinesis was blocked by adding cytochalasin B (6 μg/ml) to the cultures after 44 h of phytohemagglutinin stimulation. Cells after harvest were treated with a hypotonic solution (0.56% KCl) and fixed with methanol–glacial acetic acid (3:1). Air-dried slides were stained with 6% giemsa stain and propiodium iodide (6 μg/ml). One thousand binucleated cells were counted, following the scoring criteria adopted by the Human Micronucleus Project (Bonassi et al., 2001).

2.13. Statistical analysis

Statistical analyses were performed by one-way analysis of variance (ANOVA) followed by Dunnett's multiple comparisons test (Sigma Plot 11.0, USA). The level of statistical significance chosen was $p<0.05$, unless otherwise stated.

3. Results and discussion

The composition and properties of CFA particles changes with the quality of coal, combustion process, and precipitation technique (Celik et al., 2007). Analysis of CFA used in this study revealed the presence of various toxic heavy metals on CFA particles, and their release in ultrapure water (Aq) and DMSO media on incubation for 24 h. The data in Table 1 show the concentrations of heavy metals such as Fe, Ni, Cu and Cr as 34,160.0 ± 1.38, 150.8 ± 0.78, 99.3 ± 0.56 and 64.0 ± 0.86 μg/g CFA, respectively. These metals were released from CFA in the order Cr > Ni > Cu > Fe in CFA-DMSO extract. The amounts of Fe recovered in CFA-DMSO and -Aq extracts were found to be 210 ± 3.4 μg/g and 88.6 ± 17.9 μg/g, which is equivalent to 0.6% and 0.25%, respectively of the total Fe present on CFA. Most likely, the higher extraction efficiency of Fe in DMSO as compared to water is due to higher solubility of ferric salts in DMSO (90 g/100 ml) (http://www.gaylordchemical.com) as compared to 60 g/100 ml in water, due to the aprotic nature of the solvent. The ability of CFA to release bioavailable metals has evoked much interest in understanding the CFA-induced oxidative stress, due to the generation of oxidants through redox-cycling (Ball et al., 2000; Chen et al., 2005a). The absolute amounts of Ni, Cu and Cr in CFA-DMSO extract were found to be much lesser than the total amount of Fe present on CFA particles. However, the greater release of 67% Cr (43.30 ± 9.24 μg/g) and 3.3% Ni (5.99 ± 1.23 μg/g) in DMSO extract as compared to 0.6% iron, suggested the role of Cr and Ni in causing genotoxic effects. Linak et al. (2007) have also suggested the presence of Cr in the ultrafine ash particles through X-ray absorption fine structure (XAFS) spectroscopy. Earlier studies have demonstrated that the cells treated with Cr(VI) exhibit different types of DNA damage including base modification, single-strand breaks, double-strand breaks, Cr–DNA adducts, DNA–Cr–DNA adducts, and protein–Cr–DNA adducts (Wise et al., 2008). Moreover, Andersen (1983) suggested the Cr(III) ion as an ultimate carcinogenic form of chromium. The heavy metals associated with sub-micron (<1 μm) fractions of CFA and residual oil fly ash (ROFA) and OFA have been implicated in ROS production, expression and synthesis of the inflammatory cytokine interleukin-8 (IL-8), and lung cancer (Lay et al., 1999; Smith et al., 2000; Grimsrud et al., 2002; Di Pietro et al., 2011b). In most of the studies, the ultrafine particles of fly ash were uncharacterized and particulate size unspecified under the treatment conditions. Since, the toxicity of nanoparticles varies with size, shape and state of dispersion (Powers et al., 2007), we have characterized the CFA-NPs by use of the state-of-the-art sensitive techniques including XRD, TEM, SEM, AFM and FTIR, and assessed their genotoxic potential in Aq- and DMSO-extracts using sensitive in vitro assays.

The XRD analysis of CFA powder revealed the presence of quartz crystallite (26.62°), mullite (16.422° and 40.851°), iron oxide (33.197°) and amorphous glassy materials (36.53°) at 2θ value (Fig. 1). The average size of crystalline CFA-NPs was determined to be 14 nm, as calculated based on FWHM, using Scherrer's equation. The peaks in Fig. 1 correspond with the XRD diffractogram of ball-milled fly ash, as reported previously (Paul et al., 2007). The SEM analysis of powdered CFA in Fig. 2A, validated the presence of spherical shaped CFA particles. The TEM image provided the size range of CFA-NPs as 11–25 nm (results not shown).

Table 1
Heavy metal analysis of CFA and its Aq and DMSO extracts.

Heavy Metals	Concentration (μg/g)		
	CFA	CFA DMSO extract	CFA Aq extract
Copper	99.3 ± 0.56	1.9 ± 0.89 (1.91%)	N.D
Chromium	64.0 ± 0.86	43.3 ± 9.24 (67%)	40 ± 9.24 (62.5%)
Iron	34160.0 ± 1.38	210 ± 3.45 (0.6%)	88.6 ± 17.9 (0.25%)
Nickel	150.8 ± 0.78	5.99 ± 1.23 (3.3%)	N.D

The data represent the mean ± S.D of three independent analyses for each metal.
N.D: not detectable. Values in parenthesis indicate the % release of metals from CFA.

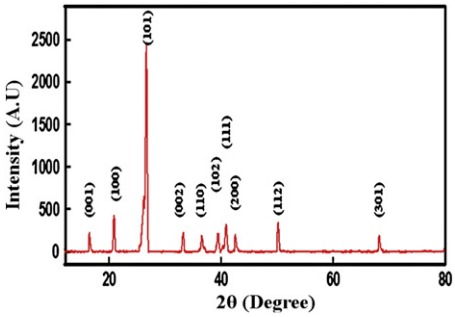

Fig. 1. X-ray powder diffraction (XRD) analysis for phase identification of CFA-NPs.

Spherical shape is normally indicative of particulates formed due to high temperature combustion through the process of nucleation, coagulation, and condensation of vaporized materials (Heasman and Watt, 1989). Such particles, generated as a result of thermal treatments are very small (0.001–10 μm) (Kimbrough, 1998). Silva et al. (2009) have also reported the nanometric-sized crystalline particles in fly ash in the size range of 10 to 100, consisting of iron-rich oxide (hematite), Fe-sulfate and Fe-aluminum silicate glass using energy-dispersive X-ray spectrometer (EDS) and high-resolution transmission electron

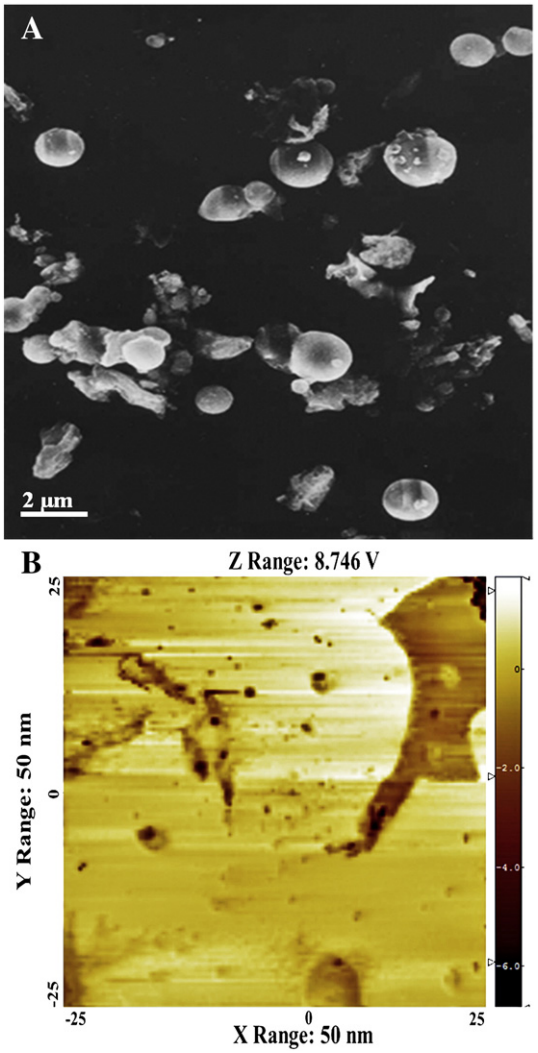

Fig. 2. Representative SEM image of CFA (panel A) at 1000× magnifications. Panel B depicts a 3D topography of CFA-NPs in an AFM perspective view. Scan size is 5 × 5 μm. The intensity of color in side bar reflects the height of the particles. (For interpretation of the references to color in this figure legend, the reader is referred to the web version of this article.)

microscopy (HR-TEM) images. Also, the complex micromineralogy of the airborne combustion-derived nanomaterials demonstrated the presence of aluminosilicate (Al–Si) glassy spheres, iron oxide nanocrystals (mainly hematite and magnetite) mixed with silicate glass particles containing potentially bioreactive transition metal (Cr, Ni) (Silva and da Boit, 2011). The AFM analysis (Fig. 2B) revealed the amorphous structures with embedded quartz crystallites of average CFA-NP size and roughness of 21 and 24 nm, respectively. This size range is in agreement with the earlier findings (Heasman and Watt, 1989; Chen et al., 2005b). Size is a key factor in determining the potential toxicity of CFA particles. Indeed, the smaller the particle, the greater is its surface area to volume ratio, and the higher its chemical reactivity and biological activity. The greater chemical reactivity of nanomaterials may result in increased production of reactive oxygen species (ROS), including free radicals (Nel et al., 2006). ROS production is one of the primary mechanisms of nanoparticle toxicity; it may result in oxidative stress, inflammation, and consequent damage to proteins, membranes and DNA (Nel et al., 2006). Indeed, the combustion-derived nanoparticles have been identified as an important component of particulate matter in inducing adverse effects on human health (Laden et al., 2000; Wichmann and Peters, 2000; Ibald-Mulli et al., 2002). Several epidemiological studies have suggested adverse reproductive effects (Lewtas, 2007), promutagenic lesions (Binkova et al., 2007), and a variety of chronic diseases (Brunekreef and Holgate, 2002; Chen et al., 2008), such as chronic obstructive pulmonary diseases (COPD) (Ling and van Eeden, 2009), lung cancer (Pope et al., 2002; Lewtas, 2007), and cardiovascular diseases (Franchini and Mannucci, 2009) upon exposure to air borne particulate matter. The most toxic component of airborne particulate is the nano-sized particles, which have unhindered access to the cells of the airway and other intracellular compartments (Donaldson et al., 2003; Gwinn and Vallyathan, 2006; Duffin et al., 2007). These nanoparticles have a potential to translocate from the site of deposition in the lungs to the blood and other target organs (Donaldson et al., 2004). The deposition of 20 nm particles is 2.7 times greater than 100 nm particles and 4.3 times greater than 200 nm particles in the lungs of healthy individuals (Stahlhofen et al., 1989). Higher deposition efficiencies occur in patients with asthma or chronic obstructive pulmonary disease than in healthy subjects, possibly due to decreased clearance ability (Anderson et al., 1990; Duffin et al., 2007). Kreyling et al. (2006) reported less than 25% clearance of 50 and 100 nm particles during the first 24 h after inhalation. The level of persistence of the inhaled particles is an important characteristic determining the degree of inflammation and tissue injury (Donaldson et al., 2004; Bonner, 2007). Furthermore, the release of surface adsorbed transition metals and organics on CFA particles can undergo chemical reactions in the milieu of the lungs leading to the production of free radicals such as superoxide anion or hydroxyl radical, as a primary pro-inflammatory mechanism (Rice et al., 2001; Squadrito et al., 2001; Baulig et al., 2003).

The FTIR data validated the presence of Si – O – Si groups of quartz in CFA. The spectrum in Fig. 3 shows typical FTIR bands at 1084.50, 783.43 and 456.85 cm^{-1}. The bands at 1084.50 and 783.43 cm^{-1} are attributed to the asymmetrical stretching vibration and symmetrical stretching vibration of the Si – O – Si groups (Thongsang and Sombatsompop, 2006). The quartz crystals are frequently found on the surface of CFA (Bai et al., 2010). Quartz has been classified as a carcinogen by IARC/WHO (1997) and has been shown to cause lung cancer (Taeger et al., 2008). Recently, Chen et al. (2010) reported that workers at the fly ash treatment plant in Taiwan had significantly higher DNA damage than those at the bottom ash recovery plant. The fine particles have been suggested to be responsible for the DNA damage in workers inhaling the metal into the human body. The particles with an aerodynamic diameter of 0.1–2 μm have good penetrability through cotton or active carbon masks and the personal protective equipments are not so effective for protecting workers against occupational hazards (Wang et al., 2006). The reported health hazards associated with the fly ash and detection of nanosized CFA particles has led us to explore the mechanistic aspects of CFA induced oxidative DNA damage in human PBMN cells. Our results

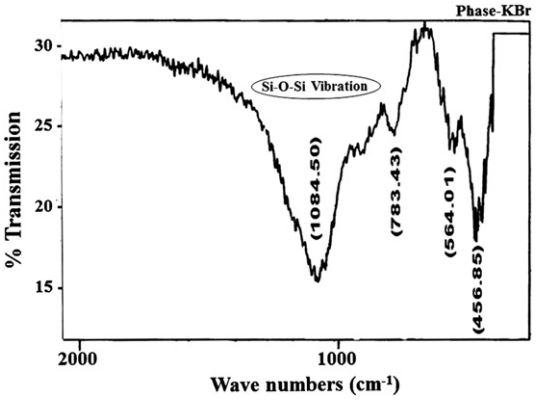

Fig. 3. Fourier Transformed Infra Red (FTIR) spectrum of CFA-NPs.

explicitly demonstrated that the generation of CFA-NPs induced ROS both extracellularly and intracellularly in PBMN cells. The absolute amounts of $O_2^{\bullet -}$ anions produced by CFA in DMSO extract upon exposure to white light in the presence of NBT were estimated to be 19.2, 21.7, 25.1, 26.5 and 36.6 μM at 100, 200, 400, 600 and 800 ppm, respectively. The amount of $O_2^{\bullet -}$ generated by CFA in the Aq-extract was relatively lesser as compared with the CFA-DMSO extract at a similar concentration range (Supplementary Fig. S1). Qualitative analysis of intracellular ROS generation revealed a concentration dependent increase in the fluorescence intensity of DCF in CFA-NPs treated cells as compared to the untreated control cells (Fig. 4A). Considering the fluorescence intensity of untreated control cells as 100%, the CFA-DMSO extract treated cells at 600, 1200 and 2400 ppm exhibited 27%, 29% and 32% higher fluorescence intensity of DCF ($p<0.05$), respectively. Cells treated separately with H_2O_2 (100 μM) and DMSO (0.5%) were taken as positive and solvent controls. Most likely, the Fe(III) associated with CFA-NPs play an important role in ROS generation and oxidative stress (Di Pietro et al., 2011a).

Furthermore, the flow data demonstrated a CFA concentration dependent reduction in the mitochondrial fluorescent intensity by 73.7%, 78.6% and 83.4% at 600, 1200 and 2400 ppm, respectively (Fig. 4B), which suggests a significant change in the mitochondrial potential ($\Delta\Psi m$). Upadhyay et al. (2003) have demonstrated that particulate matter (PM) caused dose-dependent reductions in $\Delta\Psi m$, caspase 9 activation, and apoptosis by mechanisms that involve the mitochondria-regulated death pathway and the generation of iron derived free radicals. In addition, the relationship between the exogenous oxidative insult induced by metals and the endogenous oxidative stress, elicited by electron leakage from the respiratory chain, located in the inner mitochondrial membrane (Trifunovic and Larsson, 2008), also results in abnormal concentrations of free superoxide anion ($O_2^{\bullet -}$), and H_2O_2 (Seo et al., 2008; Porcell et al., 2009). H_2O_2 is more stable than $O_2^{\bullet -}$ and, therefore, is able to diffuse freely through mitochondrial membranes, causing oxidative damage in the cytosol, as shown by an increase of ROS levels in CFA-NP treated PBMN cells.

The ct-DNA treated with CFA-Aq and -DMSO extracts exhibited a concentration dependent decrease in the fraction of duplex DNA with a concomitant increase in the degree of single strandedness in the treated ctDNA (Fig. 5). The number of breaks per unit DNA increased as 1.21, 2.07, 2.54, 2.96 and 3.6 at DNA nucleotide/CFA DMSO extract (ppm) ratio of 1:20,1:40,1:60, 1:80 and 1:100, respectively. Almost a similar dose dependent trend with lesser DNA damage was noticed with Aq-extract. At the highest DNA nucleotide/CFA ppm ratio of 1:100, about 1.8 and 3.6 strand breaks per unit of DNA were produced with CFA-Aq and -DMSO extracts, respectively (Table 2). A parallel control does not show any reduction in the amount of duplex DNA. The CFA dose-dependent DNA damage was further validated by comet assay in PBMN cells. The digitized images of representative comets clearly

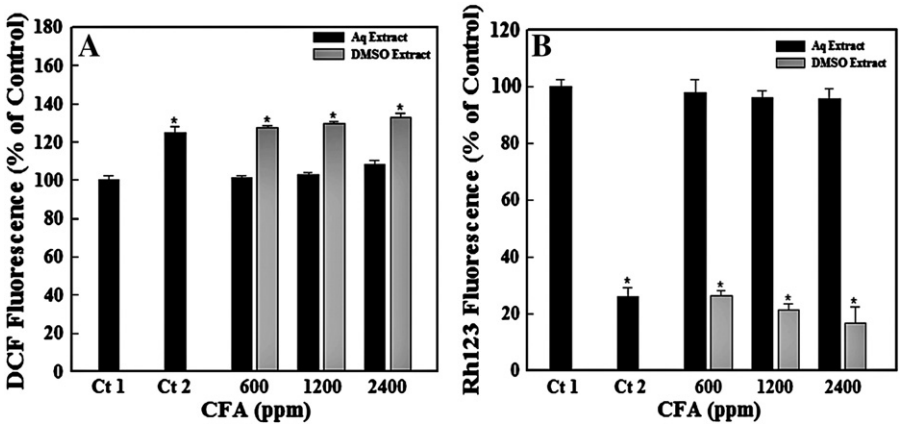

Fig. 4. CFA-NPs induced intracellular ROS production (panel A) and changes in mitochondrial membrane potential (ΔΨm) (panel B) in PBMN cells. The data represent the mean ± S.D of three independent experiments (*p<0.05 relative to control). Ct1: DMSO (0.5%) as solvent control; Ct2 : H_2O_2 (100 μM) as positive control.

demonstrate the extent of broken DNA released from the heads of the comets during electrophoresis at increasing CFA doses (Supplementary Fig. S2). A concentration dependent increase in DNA damage in terms of Olive tail moment (OTM) was observed in the range of 600 ppm to 2400 ppm of DMSO extracts, whereas, no change in OTM values observed even at the highest concentration of CFA-Aq extract. The quantitative data from a set of 150 cells at 2400 ppm of CFA-DMSO revealed 6-fold higher OTM as compared to DMSO control (Fig. 6, panel A). The heterogeneity in the distribution of DNA damage among cells is shown in Fig. 6 (panel B). The histogram shows that 100% of EMS treated cells (positive control) have tail lengths >200 μm, as compared to 100% cells of untreated controls with the tail lengths between 20 and 60 μm. At 2400 ppm, around 90% cells of CFA-DMSO treated cells exhibited tail lengths between 180 and 200 μm. However, the CFA-Aq treated cells have not shown any increase in tail length values. The data suggested a moderately higher DNA damage in CFA-DMSO extract as compared to CFA-Aq extract. The data revealed that almost 50 to 70% of cells up to 300 ppm exhibited 40–70 μm migrations of DNA. Recently, Markad et al. (2012) reported the genotoxicity of fly ash in the earthworm *Dichogaster curgensis* by comet assay. CFA-induced DNA damage in the coelomocytes was measured after 1, 7 and 14 days of oral exposure in the range of 2.5 to 40% w/w mixed with cattle manure, which is a much higher concentration range than the concentrations used in this study. Our results indicated that at CFA-DMSO extract concentrations of 1800 and 2400 ppm about 75–80% cells exhibited >200 μm of DNA fragment mobility, which was comparable to >200 μM DNA migration in the case of EMS treated cells. However, CFA-Aq extract at any concentrations did not induce significant DNA strand breaks (Fig. 6B) and the cells maintained the nuclear contents with no change in distribution pattern, as evident in Supplementary Figure S2 (panel II).

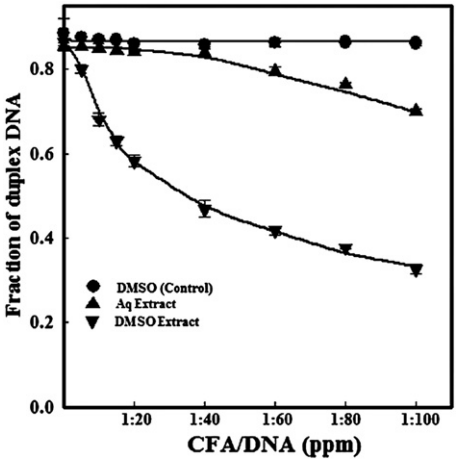

Fig. 5. CFA-Aq and -DMSO extracts induced strand breaks in ctDNA by alkaline unwinding assay. The data are mean ± SD of two independent experiments done in duplicate.

CFA induced DNA damage has been further substantiated through the formation of micronuclei in a dose-dependent manner, which is indicative of chromosomal breakage. Perhaps, this is the first report demonstrating the concentration dependent increase in the total number of BNMN in human PBMN cells upon exposure to CFA. Treatment of cells with CFA-Aq and -DMSO extracts for 24 h resulted in a significant increase ($p<0.05$) in the mean BNMN/1000 cells as validated by one-way ANOVA (Table 3). The mean BNMN with 1200 and 2400 ppm of CFA-DMSO extract were determined to be 19.0 ± 3.48 and 36.0 ± 5.65, respectively, which is about 3.8 and 6.0-fold greater than the mean BNMN cells observed with CFA-Aq extract. In addition to the formation of single micronucleus in lymphocytes, the formation of bi and multiple micronuclei were also observed in CFA-DMSO extract treated cells (Supplementary Fig. S3). This can be attributed to the direct interaction of heavy metals and the nano-sized CFA with cellular DNA, resulting in promutagenic adduct formation, which could lead to the DNA fragmentation, as a consequence of oxidative insult. Most likely, the heavy metals and organics present within and on the surface of CFA particles, may contribute substantially in free radicals generation in vicinity of DNA, which could lead to DNA damage and cellular inflammation due to oxidative stress (Saquib et al., 2012).

The data in Fig. 7 exhibited a concentration dependent increase in the levels of 8-oxodG formation in CFA-Aq and -DMSO treated ctDNA. About 3.0- and 1.97-fold increases in the levels of 8-oxodG were observed at 1000 ppm of CFA-DMSO and -Aq extracts, respectively, as compared to control. In an ex vivo study, Di Pietro et al. (2011b) also demonstrated the formation of 8-oxodG in human lymphocyte DNA

Table 2
Assessment of CFA-induced DNA strand breaks in ct-DNA by alkaline unwinding assay.

DNA/CFA ratio (v/v)	Number of breaks per unit DNA (n)	
	Aq	DMSO
Control DMSO treated DNA	N.D	N.D
Treated DNA (EMS, 1:10)	7.0	9.40
1:5	N.D	0.24
1:10	N.D	0.85
1:15	N.D	0.89
1:20	N.D	1.21
1:40	0.39	2.07
1:60	0.82	2.54
1:80	1.14	2.96
1:100	1.82	3.60

N.D: not detected.

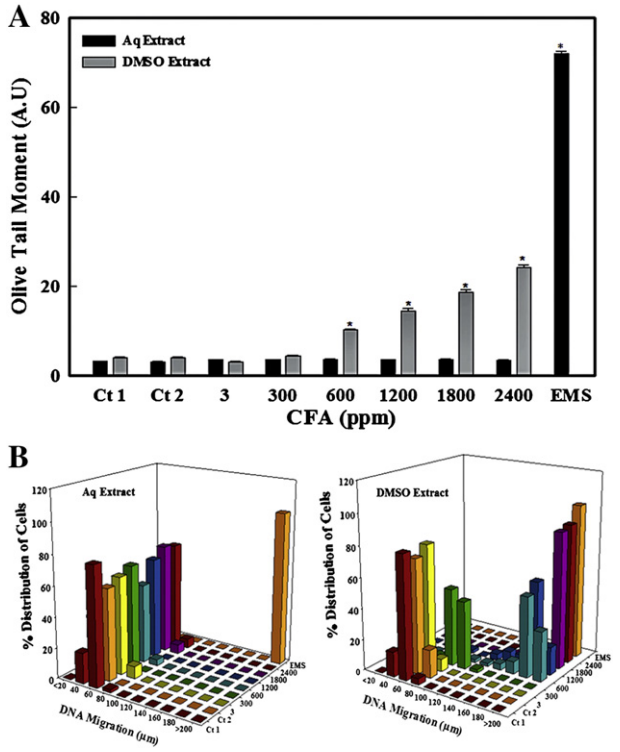

Fig. 6. DNA damage induced by CFA-Aq and -DMSO extracts in PBMN cells. Panel A shows the concentration dependent DNA damage in CFA treated PBMN cells, measured as Olive tail moment (arbitrary unit). (Panel B) Percent distribution of PBMN cells based on the extent of DNA damage. Ct1: negative control; Ct2: DMSO (0.1%) solvent control; EMS (2 mM): positive control. Each OTM histogram represents the mean ± SD value of three independent experiments done in duplicate. *$p \leq 0.05$ vs control (Ct2) based on one-way analysis of variance (ANOVA).

upon exposure with aqueous solution of OFA and observed about 7-fold inter-individual variations in the range of 8-oxodG. Also, the level of oxidative DNA damage has been reported to be significantly higher in coal miners (Schins et al., 1995). Moreover, different types of CFA containing both quartz and iron have been reported to cause cellular generation of hydroxyl radicals, oxidative DNA damage and cytotoxicity in rat lung epithelial cells (Van Maanen et al., 1999). Thus, there is a serious health hazard for workers engaged in coal-fired power plants in view of the reported association between the exposure to nano-sized coal combustion products and genetic and physiological instability leading to disorders such as lung function impairment, respiratory symptoms, mesothelioma, lung and pleural cancers (Oxman et al., 1993).

4. Conclusions

In conclusion, the assessment of the effect of CFA-NPs on ctDNA and PBMN cells provided the evidence for genotoxic potential, ascribed mainly to the bioavailable heavy metals such as Cr, Ni, and Cu in DMSO extract. The nano-sized CFA particles with surface adsorbed toxic heavy metals

Table 3
Effect of CFA-Aq and -DMSO extracts on micronucleus formation in human PBMN cells.

Variables	Concentration (ppm)	BNMN/1000 cells	
		Aq Extract	DMSO Extract
Control	0	4.0 ± 1.41	–
DMSO (%)	1.5	6.0 ± 1.38	–
MMS (μM)	100	16.0 ± 2.82*	–
CFA	600	3.0 ± 0.31	13.0 ± 3.53
	1200	5.0 ± 0.82	19.0 ± 3.48*
	2400	6.0 ± 0.58	36.0 ± 5.65*

Data are the mean ± S.D values of three independent experiments done in duplicate.
* $p<0.05$ vs. DMSO control.

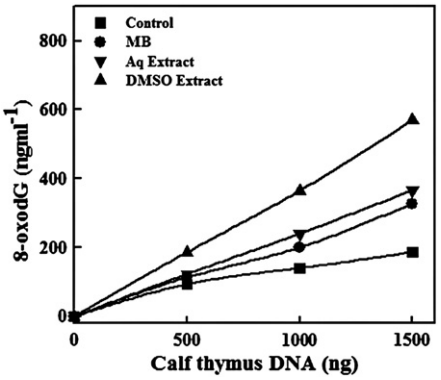

Fig. 7. ELISA based quantitative analysis of 8-oxodG DNA adduct formation in CFA treated ctDNA.

can act as putative mutagen and/or genotoxicant, capable of inducing systemic oxidative stress and DNA damage, which could serve as an initiating event in triggering process of carcinogenesis.

Supplementary data to this article can be found online at http://dx.doi.org/10.1016/j.scitotenv.2012.08.004.

Conflict of interest statement

The authors declare that there are no conflicts of interest.

Acknowledgments

The authors are thankful to King Abdulaziz City for Science and Technology (KACST), Riyadh, Saudi Arabia, for research funding under the National Plan for Science and Technology (NPST) grant no. 10-NAN1115-02. Also, the financial support through the Council for Scientific and Industrial Research, Government of India, grant no. 37(1124)/03/EMR-11, sanctioned to JM, is greatly acknowledged.

References

Adriano DC, Page AL, Elseewi AA, Chang AC, Straughan I. Utilization and disposal of fly ash and other coal residues in terrestrial ecosystem: a review. J Environ Qual 1980;9:333–44.
Ali M, Parvez S, Pandey S, Atif F, Kaur M, Rehman H, et al. Fly ash leachate induces oxidative stress in freshwater fish *Channa punctata* (Bloch). Environ Int 2004;30:993–8.
Andersen O. Effects of coal combustion products and metal compounds on sister chromatid exchange (SCE) in a macrophagelike cell line. Environ Health Perspect 1983;47:239–53.
Anderson PJ, Wilson JD, Hiller FC. Respiratory tract deposition of ultrafine particles in subjects with obstructive or restrictive lung disease. Chest 1990;97:1115–20.
Bai GI, Teng W, Wang X, Zhang H, Xu P. Processing and kinetics studies on the alumina enrichment of coal fly ash by fractionating silicon dioxide as nano particles. Fuel Process Technol 2010;91:175–84.
Ball BR, Smith KR, Veranth JM, Aust AE. Bioavailability of iron from coal fly ash: mechanisms of mobilization and of biological effects. Inhal Toxicol 2000;12:209–25.
Baulig A, Garlatti M, Bonvallot V. Involvement of reactive oxygen species in the metabolic pathways triggered by diesel exhaust particles in human airway epithelial cells. Am J Physiol Lung Cell Mol Physiol 2003;285:671–9.
Bauser HR, Bosshardt HP, Rappe C. Identification of polychlorinated dibenzop-dioxin isomers found in fly ash. Chemosphere 1978;7:165–72.
Binkova B, Chvatalova I, Lnenickova Z, Milcova A, Tulupova E, Farmer PB, et al. PAH-DNA adducts in environmentally exposed population in relation to metabolic and DNA repair gene polymorphisms. Mutat Res 2007;620:49–61.
Bonassi S, Fenech M, Lando C, et al. Human MicroNucleus Project: international database comparison for results with the cytokinesisblock micronucleus assay in human lymphocytes: I. Effect of laboratory protocol, scoring criteria, and host factors on the frequency of micronuclei. Environ Mol Mutagen 2001;37:31–45.
Bonner JC. Lung fibrotic responses to particle exposure. Toxicol Pathol 2007;35:148–53.
Brunekreef B, Holgate ST. Air pollution and health. Lancet 2002;360:1233–42.
Celik M, Donbak L, Unal F, Yuzbasioglu D, Aksoy H, Yilmaz S. Cytogenic damage in workers from a coal-fired power plant. Mutat Res 2007;627:158–63.
Chen Y, Shah N, Huggins F, Huffman GP, Dozier A. Characterization of ultrafine coalflyash particles by energy-filtered TEM. J Microsc 2005a;217:225–34.
Chen Y, Shah N, Huggins FE, Huffman GP. Transmission electron microscopy investigation of ultrafine coal fly ash particles. Environ Sci Technol 2005b;39:1144–51.
Chen H, Goldberg MS, Villeneuve PJ. A systematic review of the relation between long-term exposure to ambient air pollution and chronic diseases. Rev Environ Health 2008;23:243–97.

Chen H-L, Chen I-J, Chia T-P. Occupational exposure and DNA strand breakage of workers in bottom ash recovery and fly ash treatment plants. J Hazard Mater 2010;174:23–7.
Di Pietro A, Visalli G, Munaò F, Baluce B, La Maestra S, Primerano P, et al. Oxidative damage in human epithelial alveolar cells exposed in vitro to oil fly ash transition metals. Int J Hyg Environ Health 2009;212:196–208.
Di Pietro A, Visalli G, Baluce B, Micale R, Maestra SL, Spataro P, et al. Multigenerational mitochondrial alterations in pneumocytes exposed to oil fly ash metals. Int J Hyg Environ Health 2011a;214:138–44.
Di Pietro A, Baluce B, Visalli G, Maestrab SL, Micale R, Izzoti A. Ex vivo study for the assessment of behavioral factor and gene polymorphisms in individual susceptibility to oxidative DNA damage metals-induced. Int J Hyg Environ Health 2011b;214:210–8.
Donaldson K, Stone V, Borm PJ, Jimenez LA, Gilmour PS, Schins RP, et al. Oxidative stress and calcium signaling in the adverse effects of environmental particles (PM10). Free Radical Biol Med 2003;34:1369–82.
Donaldson K, Stone V, Tran CL, Kreyling W, Borm PJA. Nanotoxicology: a new frontier in particle toxicology relevant to both the workplace and general environment and to consumer safety. Occup Environ Med 2004;61:727–8.
Duffin R, Mills NL, Donaldson K. Nanoparticles, a thoracic toxicology perspective. Yonsei Med J 2007;48:561–72.
Franchini M, Mannucci PM. Particulate air pollution and cardiovascular risk: short-term and long-term effects. Semin Thromb Hemost 2009;35:665–70.
Fujii T, Hayashi S, Hogg JC, Vincent R, van Eeden SF. Particulate matter induces cytokine expression in human bronchial epithelial cells. Am J Respir Cell Mol Biol 2001;25:265–71.
Griffin RA, Schuller RM, Suloway JJ, Shimp NF, Childers WF, Shiley RH. Chemical and biological characterization of leachates from coal solid waste. Environmental geology notes, vol. 89. Chamaign, IL: Illinois Institute of Natural Resources, State Geological Survey Division; 1980.
Grimsrud TK, Berge SR, Haldorsen T, Andersen A. Exposure to different forms of nickel and risk of lung cancer. Am J Epidemiol 2002;156:1123–32.
Gwinn MR, Vallyathan V. Nanoparticles: health effects-pros and cons. Environ Health Perspect 2006;114:1818–25.
Heasman I, Watt J. Particulate pollution case studies which illustrate uses of individual particle analysis by scanning electron microscopy. Environ Geochem Health 1989;11:157–62.
Hirayama J, Tomaoka H, Horikoshi K. Improved immobilization of DNA to microwell plates for DNA –DNA hybridization. Nucleic Acids Res 1996;24:4098–9.
Ibald-Mulli A, Wichmann HE, Kreyling W, Peters A. Epidemiological evidence on health effects of ultrafine particles. J Aerosol Med 2002;15:189–201.
International Agency for Research on Cancer (IARC). Silica, some silicates, coal dust and para-aramid fibrils. Monograph on the evaluation of the carcinogenic risk of chemicals to humans, vol. 68. Geneva: IARC Press; 1997.
Jala S, Goyal D. Fly ash as a soil ameliorant for improving crop production — a review. Bioresour Technol 2006;97:1136–47.
Kalantzi OI, Hewitt R, Ford KJ, Cooper L, Alcock RE, Thomas GO, et al. Low dose induction of micronuclei by lindane. Carcinogenesis 2004;25:613–22.
Kalra N, Jain MC, Joshi HC, Choudhary R, Harit RC, Vatsa BK, et al. Fly ash as a soil conditioner and fertilizer. Bioresour Technol 1998;64:163–7.
Kimbrough DE. Elemental air pollution. In: Meyers RA, editor. Environmental analysis and remediation; 1998. p. 1605–12.
Kleinjans JC, Janssen YM, van Agen B, Hageman GJ, Schreurs JG. Genotoxicity of coal fly ash, assessed in vitro in Salmonella typhimurium and human lymphocytes, and in vivo in an occupationally exposed population. Mutat Res 1989;224:127–34.
Kreyling WG, Semmler-Behnke M, Moller W. Ultrafine particle–lung interactions: does size matter. J Aerosol Med 2006:1974–83.
Laden F, Neas LM, Dockery DW, Schwartz J. Association of fine particulate matter from different sources with daily mortality in six U.S. cities. Environ Health Perspect 2000;108:941–7.
Lay JC, Bennett WD, Ghio AJ, Bromberg PA, Costa DL, Kim CS, et al. Cellular and biochemical response of the human lung after intrapulmonary instillation of ferric oxide particles. Am J Respir Cell Mol Biol 1999;20:631–42.
Lewtas J. Air pollution combustion emissions: characterization of causative agents and mechanisms associated with cancer, reproductive, and cardiovascular effects. Mutat Res 2007;636:95-133.
Linak WP, Yoo J-I, Wasson SJ, Zhu W, Wendt JOL, Huggins FE, et al. Ultrafine ash aerosols from coal combustion: characterization and health effects. Proc Combust Inst 2007;31:1929–37.
Ling SH, van Eeden SF. Particulate matter air pollution exposure: role in the development and exacerbation of chronic obstructive pulmonary disease. Int J Chron Obstruct Pulmon Dis 2009;4:233–43.
Manerikar RS, Apte AA, Ghole VS. In vitro and in vivo genotoxicity assessment of Cr(VI) using comet assay in earthworm coelomocytes. Environ Toxicol Pharmacol 2008;25:63–8.
Markad VL, Kodam KM, Ghole VS. Effect of fly ash on biochemical responses and DNA damage in earthworm, Dichogaster curgensis. J Hazard Mater 2012;215:191–8.
Nel A, Xia T, Madler L, Li N. Toxic potential of materials at the nanolevel. Science 2006;311:622–7.
Oxman AD, Muir DC, Shannon HS, Stock SRT, Hnizdo E, Lanfe HJ. Occupational dust exposure and chronic obstructive pulmonary disease. Am Rev Respir Dis 1993;148:38–48.
Pandey VC, Singh N. Impact of fly ash incorporation in soil systems. Agric Ecosyst Environ 2010;136:16–27.
Parisar. ENVIS news letter, state environment related issues, Department of Forest, Ecology & Environment, Govt of Karnataka, vol. 2 No. 6. ; 2007.
Patterson AL. The Scherrer formula for X-ray particle size determination. Phys Rev 1939;56:978–82.
Paul KT, Satpathy SK, Manna I, Chakraborty KK, Nando GB. Preparation and characterization of nano structured materials from fly ash: a waste from thermal power stations, by high energy ball milling. Nanoscale Res Lett 2007;2:397–404.
Pope CA, Burnett RT, Thun MJ, Calle EE, Krewski D, Ito K, et al. Lung cancer, cardiopulmonary mortality, and long-term exposure to fine particulate air pollution. JAMA 2002;287: 1132–41.
Porcell AM, Angelin A, Ghelli A, Mariani E, Martinuzzi A, Carelli V, et al. Respiratory complex I dysfunction due to mitochondrial DNA mutations shifts the voltage threshold for opening of the permeability transition pore toward resting levels. J Biol Chem 2009;284:2045–52.
Powers KW, Palazuelos M, Moudgil BM, Roberts SM. Characterization of the size, shape, and state of dispersion of nanoparticles for toxicological studies. Nanotoxicology 2007;1:42–51.
Rice TM, Clarke RW, Godleski JJ, Mutairi EA, Jiang NF, Hauser R, et al. Differential ability of transition metals to induce pulmonary inflammation. Toxicol Appl Pharmacol 2001;177:46–53.
Saquib Q, Al-Khedhairy AA, Al-Arifi S, Dhawan A, Musarrat J. Assessment of methyl thiophanate-Cu (II) induced DNA damage in human lymphocytes. Toxicol In Vitro 2009;23:848–54.
Saquib Q, Al-Khedhairy AA, Singh BR, Arif JM, Musarrat J. Genotoxic fungicide methyl thiophanate as an oxidative stressor inducing 8-oxo-7,8-dihydro-2′-deoxyguanosine adducts in DNA and mutagenesis. J Environ Sci Health B 2010;45:40–5.
Saquib Q, Al-Khedhairy AA, Siddiqui MA, Abou-Tarboush FM, Azam A, Musarrat J. Titanium dioxide nanoparticles induced cytotoxicity, oxidative stress and DNA damage in human amnion epithelial (WISH) cells. Toxicol In Vitro 2012;26:351–61.
Schins RP, Schilderman PA, Borm PJ. Oxidative DNA damage in peripheral blood lymphocytes of coal workers. Int Arch Occup Environ Health 1995;67:153–7.
Seo AY, Xu J, Servais S, Hofer T, Marzetti E, Wohlgemuth SE, et al. Mitochondrial iron accumulation with age and functional consequences. Aging Cell 2008;7:706–16.
Silva LFO, da Boit KM. Nanominerals and nanoparticles in feed coal and bottom ash: implications for human health effects. Environ Monit Assess 2011;174:187–97.
Silva LFO, Moreno T, Querol X. An introductory TEM study of Fe-nanominerals within coal fly ash. Sci Total Environ 2009;407:4972–4.
Singh LP, Siddiqui ZA. Effects of fly ash and *Helminthosporium oryzae* on growth and yield of three cultivars of rice. Bioresour Technol 2003;86:73–8.
Singh NP, McCoy MT, Tice RR, Schneider EL. A simple technique for quantitation of low level of DNA damage in individual cells. Exp Cell Res 1988;175:184–91.
Smith KR, Veranth JM, Hu AA, Lighty JS, Aust AE. Interleukin-8 levels in human lung epithelial cells are increased in response to coal fly ash and vary with the bioavailability of iron, as a function of particle size and source of coal. Chem Res Toxicol 2000;13:118–25.
Squadrito GL, Cueto R, Dellinger B, Pryor WA. Quinoid redox cycling as a mechanism for sustained free radical generation by inhaled airborne particulate matter. Free Radic Biol Med 2001;31:1132–8.
Stahlhofen W, Rudolf G, James AC. Intercomparison of experimental regional aerosol deposition data. J Aerosol Med 1989;2:285–308.
Sushil S, Batra VS. Analysis of fly ash heavy metal content and disposal in three thermal power plants in India. Fuel 2006;85:2676–9.
Taeger D, Krahn U, Wiethege T, Ickstadt K, Johnen G, Eisenmenger A, et al. A study on lung cancer mortality related to radon, quartz, and arsenic exposures in German uranium miners. J Toxicol Environ Health A 2008;71:859–65.
Thongsang S, Sombatsompop N. Effect of NaOH and Si69 treatments on the properties of fly ash/natural rubber composites. Polym Compos 2006;27:30–40.
Tiwari S, Kumari B, Singh SN. Evaluation of metal mobility/immobility in fly ash induced by bacterial strains isolated from the rhizospheric zone of *Typha latifolia* growing on fly ash dumps. Bioresour Technol 2008;99:1305–10.
Trifunovic A, Larsson NG. Mitochondrial dysfunction as a cause of ageing. J Intern Med 2008;263:167–78.
Upadhyay D, Panduri V, Ghio A, Kamp DW. Particulate matter induces alveolar epithelial cell DNA damage and apoptosis: role of free radicals and the mitochondria. Am J Respir Cell Mol Biol 2003;29:180–7.
Van Maanen JM, Borm PJ, Knaapen A, van Herwijnen M, Schilderman PA, Smith KR, et al. In vitro effects of coal fly ashes: hydroxyl radical generation, iron release, and DNA damage and toxicity in rat lung epithelial cells. Inhal Toxicol 1999;11: 1123–41. www.rmajko.com/flyash.html (Last assessed on 9–4–2012).
Wang SM, Shih TS, Huang YS, Chueh MR, Chou JS, Chang HY. Evaluation of the effectiveness of personal protective equipment against occupational exposure to N,N-dimethylformamide. J Hazard Mater 2006;138:518–25.
Wichmann HE, Peters A. Epidemiological evidence of the effects of ultrafine particle exposure. Philos Trans R Soc Lond A 2000;358:2563–5.
Wise SS, Holmes AL, Wise JP. Hexavalent chromium-induced DNA damage and repair mechanisms. Rev Environ Health 2008;23:39–57.
Wong MH, Wong JWC. Effects of fly ash on yields and elemental composition of two vegetables, *Brassica parachinensis* and *B chinensis*. Agric Ecosyst Environ 1990;30:251–9.
Zhou JB, Wang TG, Huang YB, Mao T, Zhong NN. Size distribution of polycyclic aromatic hydrocarbons in urban and suburban sites of Beijing, China. Chemosphere 2005;61: 792–9.